Generation and characterization of erbium-Raman noise-like pulses from a figure-eight fibre laser

2015 Laser Phys. 25 045106

(http://iopscience.iop.org/1555-6611/25/4/045106)

IOP Publishing | Astro Ltd Laser Physics

Laser Phys. **25** (2015) 045106 (8pp) doi:10.1088/1054-660X/25/4/045106

Generation and characterization of erbium-Raman noise-like pulses from a figure-eight fibre laser

H Santiago-Hernandez[1], O Pottiez[1], R Paez-Aguirre[1], H E Ibarra-Villalon[2], A Tenorio-Torres[2], M Duran-Sanchez[3], B Ibarra-Escamilla[3], E A Kuzin[3] and J C Hernandez-Garcia[4]

[1] Centro de Investigaciones en Óptica (CIO), Loma del Bosque 115, Col. Lomas del Campestre, León, Gto. 37150, Mexico
[2] Universidad Autónoma Metropolitana, Azcapotzalco, Reynosa Tamaulipas, 02200 Ciudad de México, D.F., Mexico
[3] Instituto Nacional de Astrofísica, Óptica y Electrónica (INAOE), L. E. Erro 1, Sta. Ma. Tonantzintla, Pue. 72824, Mexico
[4] Departamento de Electrónica, División de Ingenierías Campus Irapuato-Salamanca, Universidad de Guanajuato, Carretera Salamanca-Valle de Santiago Km 3.5+1.8 Km, Comunidad de Palo Blanco, Salamanca, Gto. 36885, Mexico

E-mail: pottiez@cio.mx

Received 12 January 2015, revised 30 January 2015
Accepted for publication 9 February 2015
Published 10 March 2015

Abstract

We report an experimental study of the noise-like pulses generated by a ~300 m long passively mode-locked erbium-doped figure-eight fibre laser. Non-self-starting mode locking yields the formation of ns scale bunches of sub-ps pulses. Depending on birefringence adjustments, noise-like pulses with a variety of temporal profiles and optical spectra are obtained. In particular, for some adjustments the Raman-enhanced spectrum reaches a 10 dB bandwidth of ~130 nm. For the first time to our knowledge, we extract information on the inner structure of the noise-like pulses, using a birefringent Sagnac interferometer as a spectral filter and a nonlinear optical loop mirror as an intensity filter. In particular we show that the different spectral components of the bunch are homogeneously distributed within the temporal envelope of the bunch, whereas the amplitude and/or the density of the sub-pulses present substantial variations along the envelope. In some cases, the analysis reveals the existence of an intermediate level of organization in the structure of the noise-like pulse, between the ns bunch and the sub-ps inner pulses, suggesting that these objects may be even more complex than previously recognized.

Keywords: passive mode locking, noise-like pulses, pulse characterization

(Some figures may appear in colour only in the online journal)

1. Introduction

Passively mode-locked fibre lasers are simple, compact and low-cost sources that have long been studied for the generation of a wide variety of optical pulses [1–11]. In this work, due to their potential applications [1, 12–23], we focus on a fibre laser generating a complex type of pulse: noise-like pulses (NLPs). NLPs were observed recently in both normal [1, 17, 18, 23] and anomalous [12–16, 19, 20, 22] dispersion regimes of long fibre lasers. Such a pulse is a long (~ns) and compact collection of thousands of ultrashort (~sub-ps) inner pulses, with randomly varying amplitudes and durations. In spite of their stochastic nature, the global properties of NLPs, like the total duration of the bunch, its energy, or the average

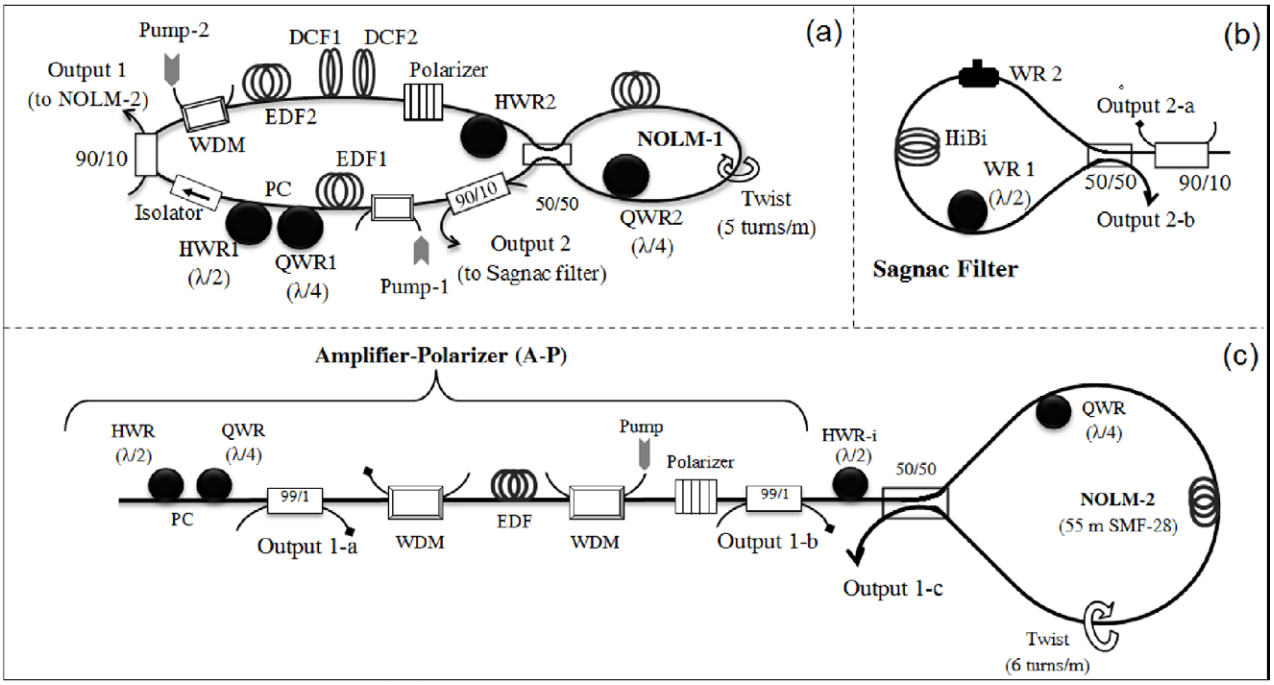

Figure 1. (*a*) Figure-eight fibre laser, (*b*) Sagnac filter, (*c*) amplifier-Polarizer stage + NOLM-2.

spectrum, are remarkably stable. Typical features of such pulses include a very large and smooth optical spectrum and a double-scaled autocorrelation, with a narrow coherence peak riding a wide pedestal. Such features make this regime easily recognizable experimentally and make it attractive for applications like sensing [24], supercontinuum generation [25–27] and data storage [28]. A review of recent literature reveals that the interest in NLPs has been expanding at a fast pace in the last few months. To give a few examples, their enhanced efficiency compared with conventional pulses for nonlinear frequency conversion has just been demonstrated [29, 30], and they are now also becoming the focus of fundamental physicists due to their possible connection with rogue waves [31, 32].

Although it is generally accepted that the NLP regime is typical of long cavities, the literature lacks unanimity on the mechanisms of formation of these pulses (random cavity birefringence [12], soliton collapse [15, 16], peak power clamping [17] and Raman scattering [33] have been invoked, among others). The diversity of models of noise-like pulsing and the fact that none of them has been ruled out so far by experimental evidence may be in part explained by the low level of information provided by standard measurements, like the autocorrelation, optical spectrum and scope traces, which only give an overall, averaged view of NLPs. Smarter measurements would help provide more decisive information regarding the mechanisms of noise-like pulsing. Precise characterization of NLPs is a challenging task however, in particular considering: (1) their fast (shot-to-shot) variation, meaning that a pulse hardly correlates with itself after each roundtrip in the cavity, and (2) their extreme complexity, with very fine (~100 fs) inner details distributed along a comparatively very long (~ns) waveform. A noticeable effort to tackle the first issue was recently reported in [34], where a pulse stretching technique was applied to provide single-shot spectral measurements. This study shows for the first time experimental evidence of some features that had been known previously mainly from numerical simulations [18], namely that NLPs are subject to large roundtrip-to-roundtrip temporal and spectral fluctuations, and that the smoothness of the trace recorded by conventional spectrum analyzers is due to strong time averaging, which irons out the spurious details. In contrast, to the best of our knowledge, no detailed study of the fine inner structure of NLPs has been reported so far.

An important category of passively mode-locked fibre lasers is known as the figure-eight laser scheme [2], in which the role of saturable absorber is played by a nonlinear optical loop mirror (NOLM) [35] or, alternatively, by a nonlinear amplifying loop mirror (NALM) [36]. Aside from conventional power-asymmetric NOLM schemes, an alternative design was proposed, which relies on a polarization imbalance [37]. As a 50/50 coupler is used, the device is power-symmetric, and polarization asymmetry is created by a quarter-wave retarder (QWR) in the loop. A polarization-dependent nonlinear phase shift then provides switching.

In this work we study NLP generation in a long figure-eight fibre laser operating in the slightly normal dispersion regime. A variety of pulse temporal envelopes and optical spectra are observed. By using a tunable periodic Sagnac filter and a nonlinear optical loop mirror at the laser output, we are able to unravel fine details of the NLPs that are not accessible through conventional measurements.

2. Experimental setup

The experimental setup is presented in figure 1. The figure-eight laser (figure 1(*a*)) is formed by a NOLM-1 (right) inserted in a ring laser cavity (left). Two 90/10 couplers provide the laser output ports. The total cavity length is ~300 m. The ring cavity

includes two sections of dispersion-compensating fibre: 100 m of DCF1 with $D = -3$ ps nm^{-1} km^{-1}, and 55 m of DCF2 with $D = -38$ ps nm^{-1} km^{-1}; the NOLM-1 is made of a 50/50 coupler, 100 m of Corning SMF-28 low birefringence fibre ($D = 17$ ps nm^{-1} km^{-1}), and a quarter-wave retarder (QWR). The net cavity dispersion is estimated to be -0.28 ps nm^{-1}. The ring also includes two sections of erbium-doped fibre (EDF) with 30 dB m^{-1} absorption at 1530 nm: 3 m EDF1 and 2 m EDF2. The EDFs are pumped at 980 nm through WDM couplers. The pump powers into EDF1 and EDF2 are ~300 mW and ~200 mW respectively. An optical isolator ensures unidirectional laser operation. The cavity also includes a polarizer and a polarization controller (PC) consisting of two retarder plates of λ/2 (HWR1) and λ/4 (QWR1), respectively. The PC is used to maximize the power transmission through the polarizer. To control the angle of linear polarization at the NOLM-1 input a half-wave retarder (HWR2) was implemented.

In the NOLM-1, a twist rate of five turns per meter is applied to the fibre, which ensures that the ellipticity of light is maintained during propagation [38]. Although the NOLM-1 shown in figure 1(*a*) is symmetric in power (a 50/50 coupler is used), a polarization imbalance is created by a QWR inserted in the loop [37]. Adjusting the orientation of the QWR2 allows for precise adjustment of the NOLM-1 low-power transmission. On the other hand, by modifying the orientation of the input polarization through the HWR2, the adjustment of the NOLM-1 switching power can be achieved [19].

A Sagnac filter and a NOLM will be used to analyze the properties of the pulses generated at the laser output. The Sagnac filter [39, 40] is shown in figure 1(*b*). It is formed by a 3 dB coupler and ~7 cm of high birefringence fibre (HiBi) that introduces a wavelength-dependent transmission, which can be adjusted using two wave retarders (WR1 and WR2). The WR1 is a half-WR obtained by coiling the fibre, and the WR2 is obtained through mechanical pressure on the fibre. The filter has a period of ~100 nm, and its transmission minima and maxima can be tuned by adjusting the angle of WR1 and the angle and pressure on WR2.

Taking advantage of the ultrafast (~fs) response time of the Kerr effect in the fibre, a NOLM was used to obtain information on the sub-ps pulses that conform the NLPs. Figure 1(*c*) shows the scheme of an amplifier-polarizer (A-P) stage and a NOLM-2 as an amplitude filter based on its nonlinear transmission. First, a PC (QWR and HWR) was used to maximize the transmission through the polarizer; subsequently, a 1.5 m, backward-pumped EDF with 1000 ppm erbium concentration was implemented to amplify the pulses from the laser output. The polarizer was used in order to ensure linear polarization at the NOLM input. In order to control the angle of linear polarization at the NOLM-2 input, a half-wave retarder (HWR-i) was implemented. The NOLM-2 is also a polarization-imbalanced scheme. It is formed by a 50/50 coupler, a QWR and a 55 m length of twisted (6 turns/m) Corning SMF-28 fibre.

3. Experimental results and discussions

For some positions of the PC, a mechanical stimulation, a kick, yields a stable mode locking operation. On the scope, mode locking is evidenced by the appearance of a stable train of pulses with a period of 1.42 μs, meaning that a single pulse circulates in the 290 m long cavity (fundamental mode locking). Once this mode is achieved, the pulse characteristics can be varied through HWR2 adjustments. For example, with such adjustments we obtained a variety of temporal profiles, as illustrated in figure 2(*a*), each profile has a different duration and shape. Several optical spectra are depicted in figure 2(*b*); in spite of their diversity, these curves are all wide and smooth, which is a typical signature of NLPs. It has to be noted that no clear correspondence was observed between each particular temporal shape and optical spectrum, in other words, different spectra sometimes correspond to similar profiles and different profiles to similar spectra. Another typical characteristic of these pulses is the double-scale autocorrelation trace depicted in figures 2(*c*) and (*d*) in the case of pulse-1 and pulse-4, respectively, with a narrow sub-picosecond peak riding a wide pedestal that extends beyond the 200 ps measurement window of the autocorrelator. We also notice that the pedestals of figures 2(*c*) and (*d*) adopt different shapes (triangular and flat, respectively): this may indicate some difference in the inner structure of these two kinds of pulses; however the autocorrelation does not provide enough information to reveal the nature of such differences. Overall, figure 2 shows that, in spite of the diversity of temporal profiles and spectra that were measured, all types of pulses generated by the mode-locked laser are NLPs.

Although the different spectra presented in figure 2(*b*) have smoothness as a common feature, they differ significantly. Indeed, HWR2 adjustments allow modification of their bandwidth over a wide range [19, 41]: considering the bandwidth at 10 dB from the maximum, it can be as small as 16 nm and as large as 130 nm, spanning between ~1550 and ~1680 nm in the case of pulse-1. Besides, as the bandwidth increases, the peak in the 1560 nm region is progressively red-shifted, it becomes increasingly asymmetric and is accompanied by a growing peak around 1660 nm. Such features are signatures of the Raman effect (including self-frequency shift), which are responsible for the extreme spectral broadening that is observed. It has been proposed in the literature that the formation of NLPs could result from the destabilization of optical pulses driven by the Raman effect [33]. This idea contrasts with that of a strong stimulated Raman scattering that stabilizes a dissipative soliton instead of destroying it [42]. The spectrum of pulse-4 in figure 2(*b*) is symmetric in the 1560 nm region and does not present any peak at 1660 nm, meaning that the Raman effect is absent in this case, whereas it is present in the other spectra, culminating in the case of pulse-1, where one can estimate that the Raman contribution amounts to ~50% of the total pulse energy. Hence we observe that, in our setup, NLPs are obtained in all cases, irrespective of the degree to which the Raman effect is present. Although the Raman effect is likely to play a role in NLP formation when it is present, these results indicate that, contrary to [33], this effect cannot be taken as the only one responsible for NLP formation in our setup. Finally, it has to be emphasized that the generation of NLPs with ~130 nm bandwidth constitutes an important achievement: although similar Raman-induced broadening

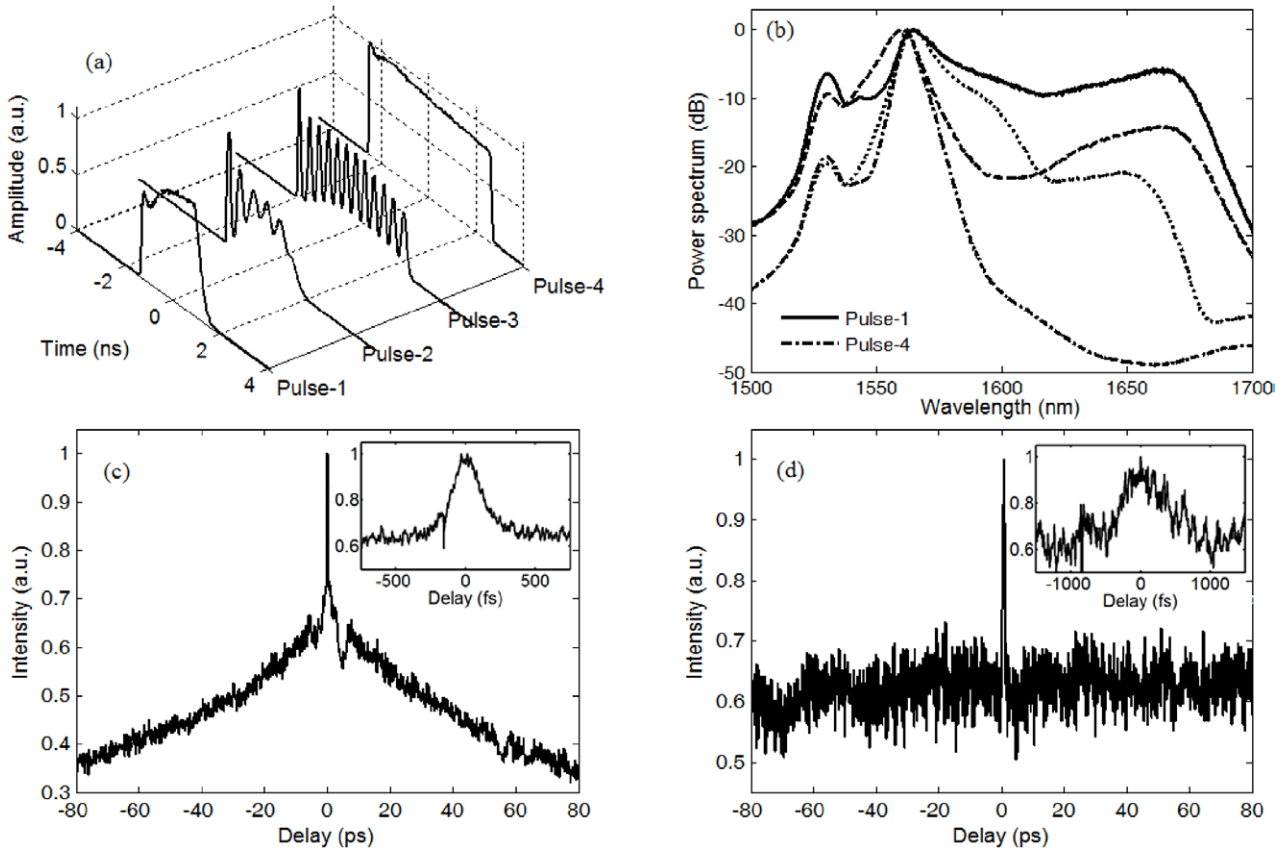

Figure 2. (*a*) Temporal profiles obtained using a 25 GHz photodetector and 50 GHz sampling scope; (*b*) optical spectra measured at output 2; (*c*, *d*) autocorrelation traces of pulse 1 and pulse 4, respectively (inset: close-up on central spur).

has been reported previously in [43] in a ring configuration, an expensive, 1 km long highly nonlinear fibre (HNLF) was required. In the present scheme, whose total length is less than 300 m, no HNLF is used, and the strong Raman broadening is believed to originate mainly from the 100 m DCF1.

Now we report the results of two different techniques to characterize NLPs. First, a Sagnac filter (figure 1(*b*)) was inserted at output 2 of the laser in order to analyze the temporal behaviour of different spectral components of the pulses. Different types of NLPs were investigated. Here we present the results for two of them: one characterized by the presence of a strong Raman component (figures 3(*a*) and (*b*)), and another one that is free of Raman contribution (figures 3(*c*) and (*d*)). In each case, by adjusting the WRs in the filter, the filter transmission was adjusted in order to select/remove different portions of the pulse spectrum. The pulse temporal envelope was then detected by the 25 GHz photodetector and monitored on the sampling scope. In figures 3(*a*) and (*b*) the dashed line corresponds to the Raman component (i.e. when the 1560 nm component is filtered away) and the dotted line shows mainly the behaviour of the 1560 nm component (although the Raman component cannot be removed completely by the filter due to its broad spectral extension, it is significantly reduced, in particular the Raman peak at 1660 nm is 10 dB below the peak at 1560 nm). For comparison, the unfiltered laser output measured at output 2-a is also shown (solid line). In the case of the Raman-free pulses, the results obtained when the red-shifted and blue-shifted components of the pulse spectrum are selected by the filter are displayed in figures 3(*c*) and (*d*). The curves of the unfiltered output are also shown as solid lines for comparison.

It can be seen from figure 3(*a*) that all profiles are very similar. The only noticeable difference appears in the temporal envelope of the Raman components (dashed curve), which is noisier and presents a small hump on the right side. It has to be noted that measurements were repeated several times in order to discard the influence of long-term drifts in the pulse shape that may take place between consecutive measurements, ensuring that the observed variation is significant. In figure 3(*c*) all of the temporal profiles are also very similar, despite the fact that filtering was applied at different sections of the optical spectrum. Similar results were obtained for all of the NLP profiles that were observed.

The optical spectra of both pulses in figures 3(*b*) and (*d*) presented a characteristic peak at ~1530 nm, which was first thought to be part of the spectrum of the NLPs. However, through the Sagnac filter we were able to filter away both the 1560 nm contribution and most of the Raman signal around 1660 nm, leaving only the 1530 nm contribution. After the removal of said peaks, we found that the pulse disappears completely on the scope, which allows the conclusion that the 1530 nm peak originates from an amplified spontaneous emission.

By filtering the spectra, we get information about the temporal distribution of different spectral components within the temporal profile of the NLPs. We observe that, for all types

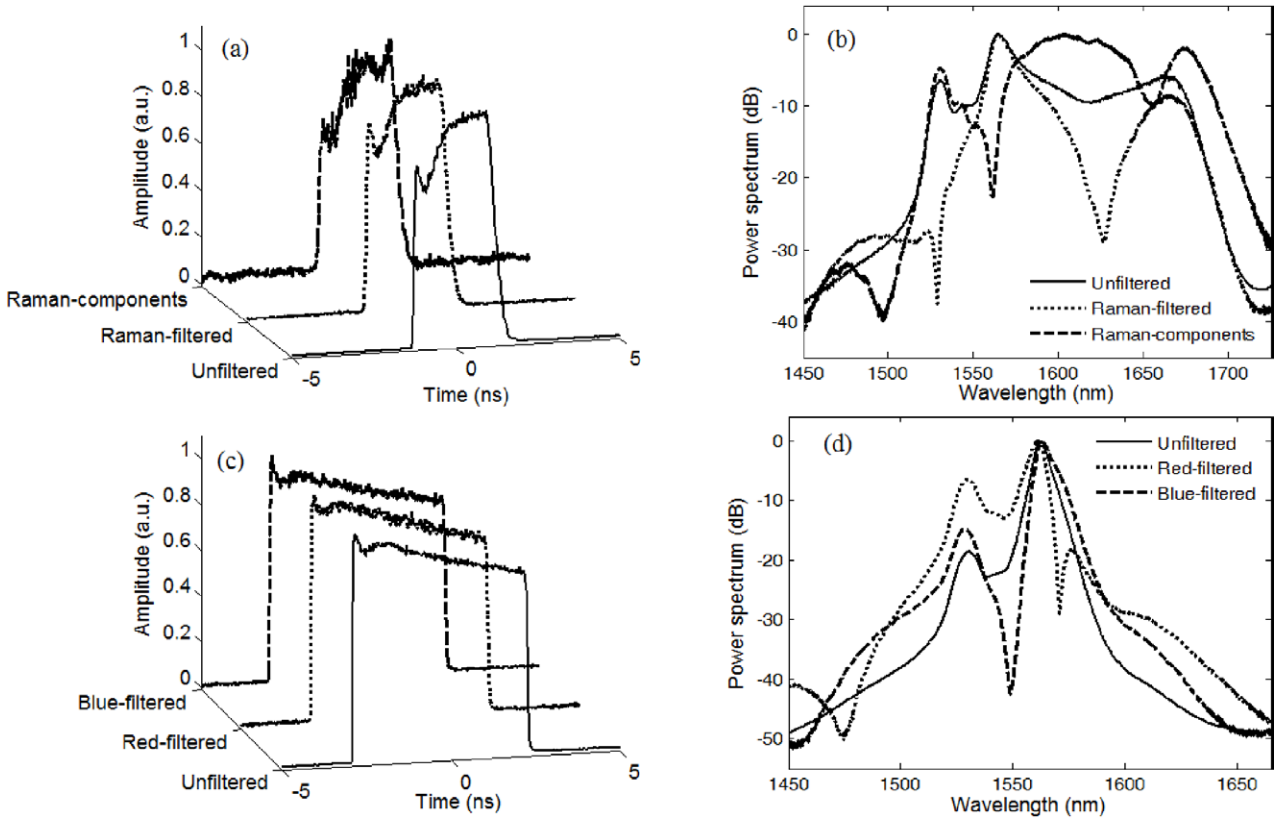

Figure 3. Measurements performed on two types of NLPs after filtering different regions of their spectra. (*a*), (*c*) Time-domain profiles of the pulses. (*b*), (*d*) Optical spectra.

of NLPs generated by the laser, the different spectral components of the pulse spectrum present very similar temporal distributions, as the corresponding profiles usually superpose with the profile of the pulse without filtering, only the envelope of the Raman-shifted components in figure 3(*a*) departs very slightly from the profile of the unfiltered pulse. Hence we conclude that there is no temporal separation within the envelope between the different spectral components of the NLP: either sub-pulses with different spectral content are distributed homogeneously within the bunch, or each of the sub-pulses contains all the spectral components present in the measured spectrum of the NLP. We believe the latter to be more likely, considering that the width of the coherence spur measured in the autocorrelation traces (a few hundred femtoseconds) yields sub-pulse durations in the order of a few 100 fs, corresponding to a bandwidth of a few tens of nm, which is consistent with the bandwidth values measured from the NLP spectra.

The A-P stage + NOLM-2 setup displayed in figure 1(*c*) is now used as an intensity filter to analyze the NLPs. This scheme was inserted at output 1 as it yields the highest laser output power. It has to be noted however that the Raman peak at 1660 nm is never present at output 1 as it lies beyond the spectrum of amplification of EDF1. The QWR and HWR-i of NOLM-2 were adjusted for minimum low-power transmission (when the laser is operated in a continuous wave) and maxum high-power transmission (using the laser in pulsed mode with maximal amplification). The nonlinear transmission characteristic of NOLM-2 was measured by using the initial maximum presented by the temporal profile depicted in the inset of figure 4(*a*). Input power to the NOLM-2 was varied by adjusting the EDF pump power of figure 1(*c*), and was measured at the 1% output of a 99/01 coupler inserted at the NOLM-2 input (output 1-b in figure 1(*c*)), and the output power was measured through the amplitude on the sampling scope of the initial maximum of the pulse at output 1-c. The results are displayed in figures 4(*a*) and (*b*). Said curves indicate a nonlinear dependence, the best fit using a cosine function (solid line in figure 4(*b*)) is obtained for: $T = 0.6815\,(\mathrm{mV}/\mu\mathrm{W}) * [1 - \cos(\pi * P_{\mathrm{in}}/550\,\mu W)]$, where P_{in} is the NOLM input power. Although for most measurements the switching power was not reached, the experimental data of figure 4(*b*) show that this power was reached (and possibly even slightly exceeded) in this case. Over the range of input power covered in this experiment, and for the previously mentioned WR adjustments, the transmission of NOLM-2 grows monotonically with power, so that it can be used like an amplitude filter, attenuating signals with small intensities and transmitting high-intensity signals.

Two representative temporal profiles of NLPs are studied as shown in figure 5. Figures 5(*a*) and (*b*) show the temporal profiles measured at output 1-b and at output 1-c (input and output of NOLM-2, respectively), where differences in the envelope profiles can be noted. In figure 5(*a*), the valley at the output is deeper than the valley at the input. Besides, the right side of the temporal profile at the output is steeper than at the input. In figure 5(*b*) we also notice differences in amplitude: in this case the valleys at the input are deeper than at the

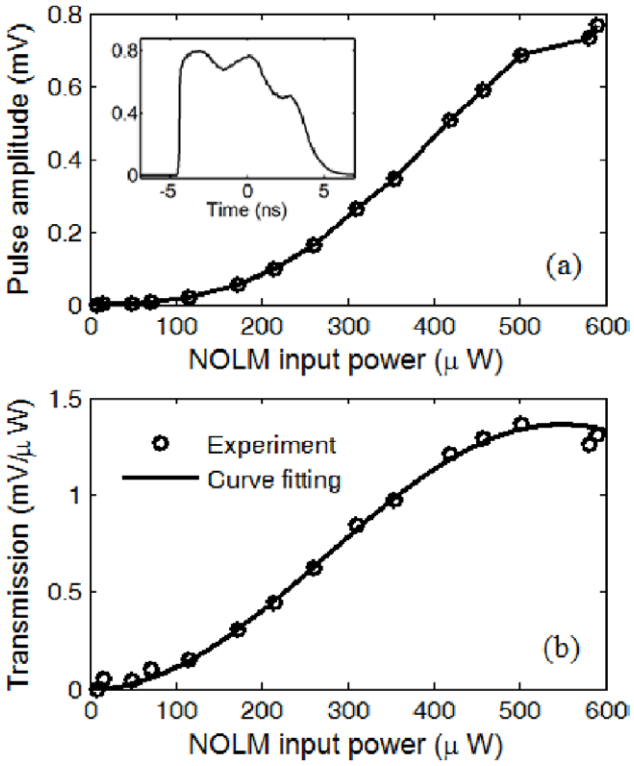

Figure 4. Measurement of NOLM-2 nonlinear transmission: (*a*) nonlinear curve of NOLM-2 output amplitude (inset: pulse temporal profile); (*b*) transmission versus input power.

output. The optical spectra at the NOLM input and output for both pulses are very similar (insets).

Considering the 25 GHz bandwidth of the photodetector and sampling scope (~40 ps response time) and assuming that NLPs are made up of densely packed sub-pulses with ~100 fs duration, the variations in the amplitude of the pulse envelopes observed in figures 5(*a*) and (*b*) must be interpreted as slow temporal variations in the average energy of the subsets of sub-pulses in the bunch, each of them encompassing a few hundreds of sub-pulses. These collective energy variations observed experimentally can have different causes: they can be due to variations in the energy (intensity and/or duration) of the sub-pulses, or to changes in the number of sub-pulses included in each subset, i.e. in the 'density' of these sub-pulses.

The results of figure 5(*a*) show that the contrast between the high- and low-amplitude portions of the envelope is increased through the NOLM, supporting the conclusion that, for this profile, the envelope reflects temporal variations in the intensity of the sub-pulses in the bunch. Indeed, with a characteristic curve such as the one displayed in figure 4(*b*), the NOLM transmission is higher for high-intensity sub-pulses and lower for low-intensity sub-pulses, yielding an enhanced intensity contrast between sub-pulses at the output. Hence, we conclude that, on average, lower-intensity sub-pulses are concentrated in the low-amplitude sections of the envelope of figure 5(*a*) (the valley on the left side and the right edge), whereas higher-intensity sub-pulses concentrate mainly at the two peaks of the envelope.

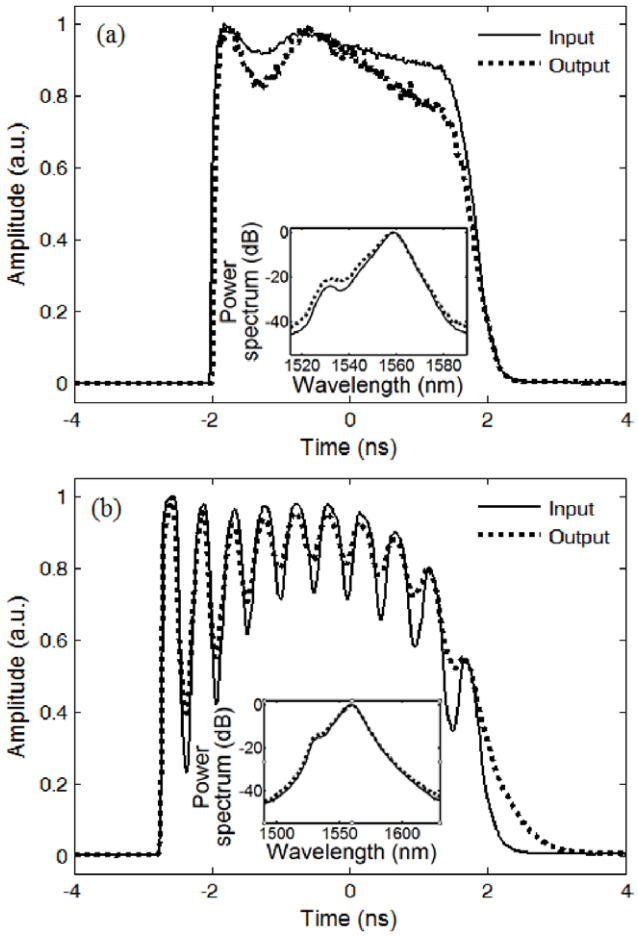

Figure 5. (*a*), (*b*) comparison between oscilloscope traces at the input and output of NOLM-2 for two different profiles (amplitude normalized to 1); inset: optical spectra.

On the other hand, figure 5(*b*) shows that the contrast between the successive peaks with different amplitudes is conserved (neither enhanced nor reduced) at the NOLM output. This confirms that the sub-pulses located at those peaks undergo the same transmission through the NOLM, meaning that, on average, they have the same intensity. Assuming that the sub-pulses have similar durations on average, the difference in amplitude between those peaks can then be accounted for by differences in the density of the sub-pulses: sub-pulses are thus more densely packed under higher-amplitude peaks of the envelope than under low-amplitude peaks. Finally, figure 5(*b*) also shows that the contrast between peaks and valleys reduces through the NOLM, meaning that the valleys undergo higher transmission through the NOLM than the peaks. Similarly, we conclude that the sub-pulses are more densely packed under the peaks than under the valleys, whereas the higher transmission of the valleys may indicate that the sub-pulses have a higher intensity in the valleys than at the peaks.

To ensure that the observed alterations of the profiles are due to the NOLM switching characteristic, and not to pulse distortions due to propagation through the EDF, polarizer and dispersive and nonlinear fibre, we replaced the NOLM-2 by a 55 m length of twisted fibre in the scheme of figure 1(*c*), and

we measured the optical autocorrelation and temporal envelope of the input and output pulses. The results indicated that the input and output temporal envelopes were identical and that the autocorrelation traces were similar, with a 30–40% increase in the width of the coherence spike at the output; this demonstrates that pulse distortion through the setup of figure 1(*c*) is moderate and cannot be responsible for the profile differences observed in figure 5.

Noise-like pulsing is a particularly complex and puzzling type of collective pulse dynamics taking place in passively mode-locked fibre lasers. Other multiple pulse behaviours like soliton crystals, soliton gases, etc, have also been evidenced and studied in such lasers [44], in which mostly identical, energy-quantified solitons are at play. Even if a condensed phase of solitons is formed, individual pulses can often still be identified using fast detection electronics [45]. In the case of a soliton gas, pulses are randomly distributed in time and drift in a disordered way, albeit slowly, at the scale of many roundtrips; hence such dynamics can easily be recorded and usually can even be observed directly on the scope. In contrast, NLPs are much more compact objects, made up of very densely packed ~100 fs pulses, which rules out any detailed direct measurement using ultrafast electronics. Besides, their dynamics are by far more chaotic, in the sense that not only the position, amplitude and energy of the sub-pulses vary, but new sub-pulses are being created and other destroyed continuously along the cavity. The fact that the inner structure of NLPs is so fine and changes so dramatically and so fast explains why it escapes most measurement methods, which considerably complicates the study of these pulses.

In spite of these difficulties, the average measurements performed and analyzed in this section trigger some interesting reflections. Particularly appealing is the discovery that, in the case of the multi-peaked waveforms of pulses 2 and 3 in figure 2(*a*), and figure 5(*b*), the slow (~ns) variations of the pulse envelope do not only map variations of the sub-pulse energy, but also of the density of these sub-pulses, across the temporal profile. More specifically, the sub-pulses are tightly packed under the peaks, but appear to be sparser under the valleys. Such sub-pulse distribution bears some analogies with the case of soliton rain/release of solitons dynamics [45], in which a condensed phase of solitons coexists with a phase of loose, widely spaced solitons that slowly drift towards/away from the condensed phase. Similarly, the peaks of the multi-peaked temporal profiles observed in this work could correspond to a series of roughly similar and equidistant packets or 'condensed phases', made up of densely packed sub-pulses. The valleys could then be interpreted as more scarcely populated intervals in which the sub-pulses that are continuously released from one packet quickly drift towards the next one, forming in each moment a pattern of more widely separated, scattered sub-pulses. Alternatively, the valleys could appear as the result of small random variations in the temporal positions of the condensed phases over successive roundtrips. As the dense packets jitter around their mean position, the sub-pulses at their edges intermittently appear in the valleys; after averaging over many thousands of pulses, the reduced likelihood of their presence in the valleys translates into the low amplitude of the envelope at those locations. The pronounced slope of the pedestal in some autocorrelation traces, as shown in figure 2(*c*), is indicative of the existence of such dense sub-ns pulse packets in some kinds of NLPs, even when peaks and valleys are not visible in the pulse envelope, (see pulse-1 in figure 2(*a*)), presumably due to strong jitter. A more accurate determination of the dynamics of NLP formation and the physical mechanisms underlying it will require further investigation and will be the focus of our future research activities.

4. Conclusions

In this work we experimentally studied NLP generation from a 290 m long, dispersion-managed passively mode-locked figure-eight fibre laser including a polarization-imbalanced NOLM. Through this setup, a stable though non-self-starting fundamental mode locking is readily obtained, yielding the formation of broadband, ns-duration NLPs with sub-ps coherence. Birefringence adjustments yield a wide variety of temporal pulse profiles and optical spectra. When the Raman effect is exploited, a smooth spectrum with a 10 dB bandwidth as large as 130 nm is readily obtained. However noise-like pulsing is also observed in total absence of the Raman effect, showing evidence that this effect is not relevant for *all* kinds of noise-like pulsing dynamics. This work also includes an analysis of the inner structure of NLPs, using a birefringent Sagnac interferometer as a spectral filter and a NOLM as an intensity filter. It was shown that the different spectral components of the NLPs are homogeneously distributed along their temporal envelope. In contrast, the amplitude and/or the density of the sub-pulses present significant variations across the pulse profile. For a particular category of NLPs, this analysis evidenced an intermediate level of organization within the waveform: the NLP is composed of a series of sub-ns packets, which themselves are made of thousands of densely packed sub-ps pulses. These results will be useful to shed light on possible scenarios of NLP formation in passively mode-locked fibre lasers and their dynamics.

Acknowledgment

This work was funded by CONACyT Project 130966.

References

[1] Zaytsev A K, Lin C H, You Y J, Tsai F H, Wang C L and Pan C L 2013 *Laser Phys. Lett.* **10** 45104
[2] Duling I N III 1991 *Opt. Lett.* **16** 539–41
[3] Matsas V J, Richardson D J, Newson T P and Payne D N 1993 *Opt. Lett.* **18** 358–60
[4] Tamura K, Ippen E P, Haus H A and Nelson L E 1993 *Opt. Lett.* **18** 1080–2
[5] Ilday F O, Buckley J R, Clark W G and Wise F W 2004 *Phys. Rev. Lett.* **92** 213902
[6] Komarov A, Amrani F, Dmitriev A, Komarov K and Sanchez F 2013 *Phys. Rev.* A **87** 23838
[7] Kobtsev S M, Kukarin S V, Smirnov S V and Fedotov Y S 2010 *Laser Phys.* **20** 351–6

[8] Lecaplain C and Grelu P 2013 *Opt. Express* **21** 10897–902
[9] Likhachev M E, Aleshkina S S and Bubnov M M 2014 *Laser Phys. Lett.* **11** 125104
[10] Lin H, Guo C, Ruan S and Yang J 2014 *Laser Phys. Lett.* **11** 085102
[11] Yun L 2013 *Laser Phys.* **13** 045106
[12] Horowitz M, Barad Y and Silberberg Y 1997 *Opt. Lett.* **22** 799–801
[13] Horowitz M and Silberberg Y 1998 *IEEE Photon. Technol. Lett.* **10** 1389–91
[14] Kang J U 2000 *Opt. Comm.* **182** 433–6
[15] Tang D Y, Zhao L M and Zhao B 2005 *Opt. Express* **13** 2289–94
[16] Zhao L M and Tang D Y 2006 *Appl. Phys.* B **83** 553–7
[17] Zhao L M, Tang D Y and Wu J 2007 *Opt. Express* **15** 2145–50
[18] Kobtsev S, Kukarin S, Smirnov S, Turitsyn S and Latkin A 2009 *Opt. Express* **17** 20707–13
[19] Pottiez O, Grajales-Coutiño R, Ibarra Escamilla B, Kuzin E A and Hernandez-Garcia J C 2011 *Appl. Opt.* **50** E24–31
[20] Vazquez-Zuniga L A and Jeong Y 2012 *IEEE Photon. Technol. Lett.* **24** 1549–51
[21] Boucon A, Barviau B, Fatome J, Finot C, Sylvestre T, Lee M W, Grelu P and Millot G 2012 *Appl. Phys.* B **106** 283–7
[22] Pottiez O, Martinez-Rios A, Monzon-Hernandez D, Salceda-Delgado G, Hernandez-Garcia J C, Ibarra-Escamilla B and Kuzin E A 2013 *Laser Phys.* **23** 035103
[23] Pottiez O, Ibarra-Escamilla B, Kuzin E A, Hernandez-Garcia J C, Gonzalez-Garcia A and Duran-Sanchez M 2014 *Laser Phys.* **24** 015103
[24] Dennis M L, Putnam M A, Kang J U, Tsai T-E, Duling I N III and Friebele E J 1997 *Opt. Lett.* **22** 1362–4
[25] Takushima Y, Yasunaka K, Ozeki Y and Kikuchi K 2005 *Electron. Lett.* **41** 399–400
[26] Hernandez-Garcia J C, Pottiez O and Estudillo-Ayala J M 2012 *Laser Phys.* **22** 221–6
[27] Zaytsev A K, Lin C H, You Y J, Chung C C, Wang C L and Pan C L 2013 *Opt. Express* **21** 16056–62
[28] Keren S, Brand E, Levi Y, Levit B and Horowitz M 2002 *Opt. Lett.* **27** 125–7
[29] Smirnov S V, Kobtsev S M and Kukarin S V 2014 *Opt. Express* **22** 1058–64
[30] Kobtsev S, Kukarin S, Smirnov S and Ankudinov I 2014 *Opt. Express* **22** 20770–5
[31] Lecaplain C and Grelu Ph 2014 *Phys. Rev.* A **90** 13805–8
[32] Runge A F J, Aguergaray C, Broderick N G R and Erkintalo M 2014 *Opt. Lett.* **39** 319–22
[33] Aguergaray C, Runge A, Erkintalo M and Broderick N G R 2013 *Opt. Lett.* **38** 2644–6
[34] Runge A F J, Aguergaray C, Broderick N G R and Erkintalo M 2013 *Opt. Lett.* **38** 4327–30
[35] Doran N J and Wood D 1988 *Opt. Lett.* **13** 56–8
[36] Fermann M E, Haberl F, Hofer M and Hochreiter H 1990 *Opt. Lett.* **15** 752–4
[37] Kuzin E A, Korneev N, Haus J W and Ibarra-Escamilla B 2001 *J. Opt. Soc. Am. B* **18** 919–25
[38] Tanemura T and Kikuchi K 2006 *J. Light. Technol.* **24** 4108–19
[39] Fang X and Claus R O 1995 *J. Opt. Lett.* **20** 2146–8
[40] González-García A, Pottiez O, Grajales-Coutiño R, Ibarra-Escamilla B and Kuzin E A 2010 *J. Laser Phys.* **20** 720–5
[41] Pottiez O, Ibarra-Escamilla B, Kuzin E A, Hernandez-Garcia J C, Gonzalez-Garcia A and Durán-Sánchez M 2014 *Laser Phys.* **24** 105104
[42] Bednyakova A E, Babin S A, Kharenko D S, Podivilov E V, Fedoruk M P, Kalashnikov V L and Apolonski A 2013 *Opt. Express* **21** 20556–64
[43] North T and Rochette M 2013 *Opt. Lett.* **38** 890–2
[44] Amrani F, Haboucha A, Salhi M, Leblond H, Komarov A and Sanchez F 2010 *Appl Phys* B **99** 107–14
[45] Chouli S and Grelu P 2010 *Phys. Rev.* A **81** 063829